Nanoscale

PAPER

View Article Online
View Journal | View Issue

Cite this: *Nanoscale*, 2025, **17**, 1326

Self-powered triboelectric sensor using GaN nanowires and stress concentration structure

Siyun Noh, Jaehyeok Shin, Seunghwan Jhee, Sumin Kang, Yumin Lee and Jin Soo Kim *

Received 8th August 2024,
Accepted 21st November 2024

DOI: 10.1039/d4nr03260h

rsc.li/nanoscale

Rapid advances in the internet of things have created various platforms for health monitoring, wearable devices, electronic skins, and smart robots. Practical realization of these new technologies inevitably requires a power supply. In this paper, we report self-powered triboelectric sensors (TESs), which incorporate GaN nanowires (NWs) grown on a Si(111) substrate as an active medium, and which are inspired by the structure of the human epidermis and dermis. The TESs were fabricated by stacking polydimethylsiloxane (PDMS) directly on GaN NWs on Si(111) and the formation of an electrode underneath the substrate. The PDMS layer forms interlocked nanoridge structures, which mimic the structure of the interface between the human epidermal and dermal layer, at the interface with the top surface of the GaN NWs. The interlocked nanoridge structures efficiently induce the transmission of stress to the underlying NWs, resulting in high triboelectric charge density and voltage. When the top surface of the TES was touched with a human finger, in the absence of an external power supply, maximum output voltage and power density of 14.7 V and 63.7 mW m^{-2} were measured, respectively. These outputs are much higher than any of those that were previously reported.

Introduction

Recent significant interest in the internet of things (IoT) has boosted the rapid development of wearable and skin-attachable electronic systems,[1–3] including artificial skins,[4,5] and systems that support human–machine interaction.[6,7] The practical application of wearable electronics requires reliable and human-friendly electronic devices and sensors to be convenient and comfortable to use. Even though considerable progress has been made in wearable platforms integrated with flexible, stretchable, and sustainable power systems, energy storage systems are still premature and unsuitable for practical use because of their impermanent lifetime, limited capacity, and questionable safety. In this regard, self-powered devices have significant potential to address the power requirements of wearable or attachable electronics. These devices generate power by harvesting energy from ambient sources such as the kinetic energy resulting from human motion. Accordingly, the development of self-powered touch sensors to meet practical applications has become one of the main new research topics in recent years.[8,9]

Department of Electronic and Information Materials Engineering, Division of Advanced Materials Engineering, and Research Center of Advanced Materials Development, Jeonbuk National University, Jeonju 54896, Republic of Korea. E-mail: kjinsoo@jbnu.ac.kr

Based on previous reports, touch sensors can be categorized into three types based on their working mechanisms: piezoresistive,[10,11] capacitive,[12,13] and piezoelectric.[14,15] Touch sensors working with the piezoresistive and capacitive types usually have high sensitivity and low detection limits.[16,17] However, an external power supply is essential to operate both of these types of sensors, which crucially limits the working environment and practicality. Piezoelectric touch sensors, on the other hand, have the advantage of self-powered operation under externally applied pressure.[14,15] However, piezoelectric touch sensors typically have low sensitivity and can only be fabricated from a limited variety of sensing materials.[18] In view thereof, it is appropriate to suggest an alternative sensing mechanism that would ensure high performance in terms of the sensitivity, yet would be highly affordable, to meet the requirements without using an external power supply. To address the technical bottlenecks, an alternative sensing mechanism has emerged in the form of the triboelectric effect, which efficiently converts external mechanical energy into electricity by harnessing contact electrification and electrostatic induction. This phenomenon enables a self-powered touch sensor to be operated effectively with high sensitivity and wearability. Triboelectric sensors (TESs) are often produced from organic materials because of their low cost and simple fabrication process.[4,5] For instance, J. Wang *et al.* demonstrated a self-powered TES based on polydimethylsiloxane (PDMS).[19] However, reliable long-term operation presented a challenge,

because the device was easily affected by external heat or humidity. Inorganic materials are not as widely used for TESs as organic materials because they complicate the device fabrication. Yet, inorganic materials have attractive characteristics for TESs including high thermal stability, high resistance to irradiation, and low impedance. TESs based on inorganic perovskite materials such as $CsPbBr_3$ and $MAPbI_3$ were reported.[20,21] However, the disadvantages of the perovskite material system are its vulnerability to moisture, long-term instability, and, in particular, the harmful substances such as lead as one of its core materials.

An alternative possibility would be to use inorganic III-nitride semiconductors. These materials are highly promising for application in TESs due to their intrinsic spontaneous polarization originating from their wurtzite (WZ) crystal structure and they offer good mechanical and chemical stability.[22] In particular, the nanowire (NW) structure is promising because it is highly likely to induce high charge density on the surface and to efficiently separate these charges spatially, compared to bulk and thin films.[23,24] However, considering that the growth of high-crystalline III-nitride NWs remains challenging,[25,26] TESs using III-nitride NWs have rarely been reported.

In this paper, we report self-powered TESs fabricated with GaN NWs and PDMS, a structure that adopts the interlocked nanoridge structure inspired by the structure of human skin. The TESs were fabricated by stacking a layer of PDMS directly on the GaN NWs grown on a Si(111) substrate. The PDMS layer forms interlocked nanoridge structures at the interface with the top surface of the GaN NWs, thereby mimicking the structure of human epidermal and dermal skin. The interlocked nanoridge structure facilitates the transmission of stress to the underlying NWs to generate high triboelectric charge density and voltage due to the spatial difference in the elastic moduli between the PDMS and NWs.

Experimental methods

GaN NWs were grown on a Si(111) substrate using a plasma-assisted molecular-beam epitaxy system equipped with a N-plasma source and effusion cells. The Si(111) substrate was chemically cleaned using a $HCl : H_2O_2 : H_2O$ solution before it was loaded into the vacuum chamber (pre-cleaning process). The pre-cleaning process was followed by *in situ* thermal annealing at a substrate temperature of 900 °C to remove the oxidation layer that naturally forms on the Si(111) substrate. Prior to growing the GaN NWs, the Si(111) substrate was exposed to the N-plasma at a substrate temperature of 800 °C to form a SiN_x layer. Subsequently, a Ga flux was supplied only to the SiN_x/Si(111) substrate for a few seconds to form Ga droplets for growth initiation. Thereafter, Ga and N-plasma fluxes were simultaneously supplied to form the GaN NWs. The growth conditions for the GaN NWs are detailed in our previous reports.[27,28]

The structural characterization of the GaN NWs was accomplished using field-emission scanning-electron microscopy (FE-SEM, Hitachi S-4700), installed in the Future Energy Convergence Core Center at Jeonbuk National University, aberration-corrected transmission-electron microscopy (Cs-TEM, Jeol Jem-Arm 200F), and X-ray diffraction (XRD, Bruker D8 Advance). For photoluminescence (PL) measurements, a diode-pumped solid-state laser with a wavelength of 266 nm was used as the excitation source, with a 0.5 m monochromater. A charge-coupled device was used to detect luminescence from the NW sample. The electrical characteristics of the TESs including the output voltage and power density were measured by varying the load resistances ranging from 1 kΩ to 1 GΩ with a Keithley 2400 source meter.

Results and discussion

Fig. 1a shows three-dimensional and plan-view (inset) FE-SEM images of GaN NWs. The average height (diameter) and spatial density of the GaN NWs were measured to be 688.7 ± 47.3 nm (71.3 ± 5.7 nm) and 4.2×10^9 cm^{-2}, respectively. The quantitative values of the GaN NWs were calculated using the Image J software installed in the FE-SEM. The surfaces of the GaN NWs shown in the FE-SEM image have hexagonal shapes, which is evidence of the formation of GaN NWs with the WZ crystal structure. Fig. 1b shows the cross-sectional (left) and high-resolution (middle) TEM (HR-TEM) images, and a selective-area electron diffraction (SAED) patterns (right), which were acquired at two different vertical positions along a single GaN NW. The lattice parameter value of 5.18 Å is in good agreement with the literature.[29] In addition, the HR-TEM images measured at the top and bottom regions of a NW revealed that defects and stacking faults, which are typically observed for compound semiconductor NWs formed on a Si substrate, were largely absent. The SAED pattern of the GaN NWs is representative of the WZ crystal structure. Fig. 1c shows the XRD rocking curve of the GaN NWs. The strong peaks at 28.32 and 58.78° correspond to Si(111) and Si(222), respectively. The peaks at 34.6 and 72.9° are attributed to the GaN(0002) and GaN(0004) planes, respectively. The full-width at half-maximum (FWHM) of the GaN(0002) and GaN(0004) peaks was measured to be 0.18 and 0.31°, respectively, and are relatively narrower compared to those of previously reported GaN NWs.[30,31] Fig. 1d shows the PL spectrum of the GaN NWs measured at room temperature (RT). The acquisition of a free-exciton (FX) peak from III-nitride nanostructures at RT is typically difficult because of the considerable number of defects and stacking faults as well as electron–phonon interaction.[32,33] In contrast, the GaN NWs fabricated in this work gave rise to a well-resolved FX peak at the wavelength of 366.3 nm at RT. These results indidcate the successful formation of highly crystalline GaN NWs.

Fig. 2 schematically presents the fabrication process of the TES using GaN NWs and PDMS, with the GaN NWs being the main response medium for the TESs. The PDMS serves as a passivation layer for the triboelectric devices and enhances their flexibility and biocompatibility. In addition, PDMS forms

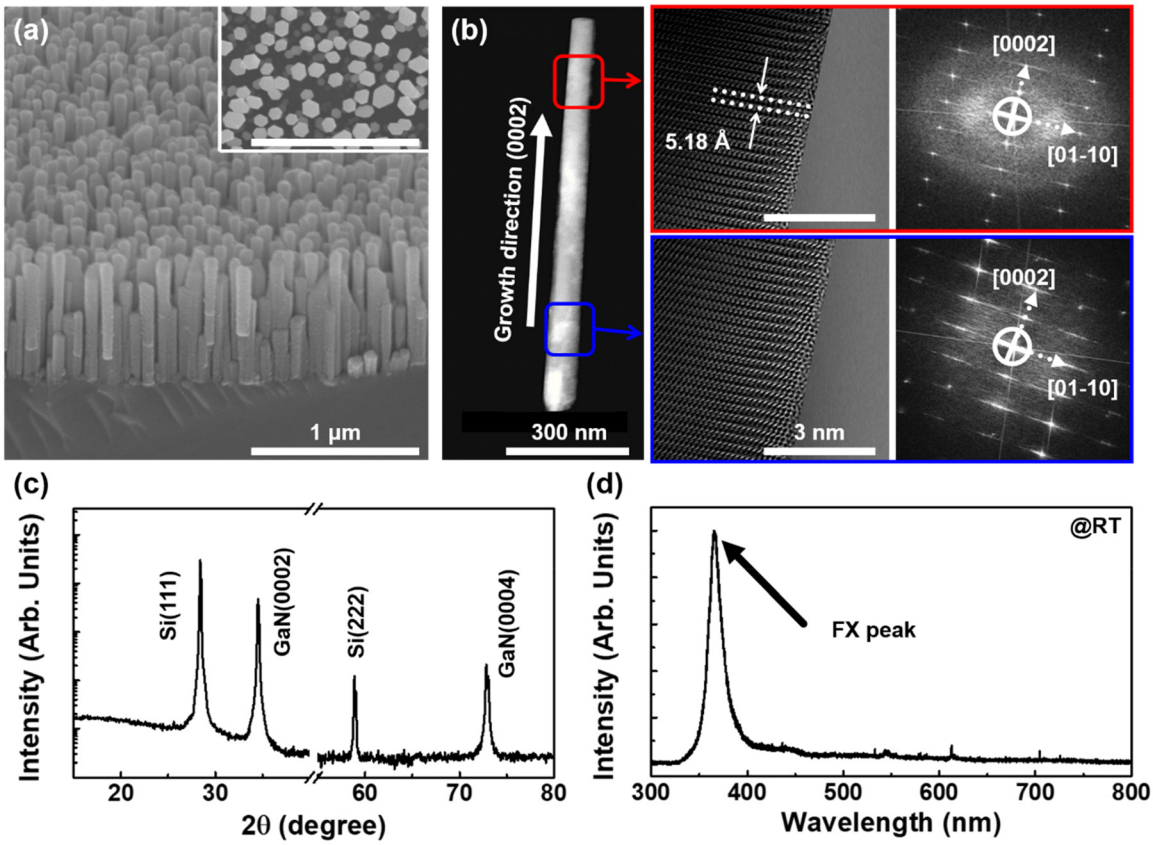

Fig. 1 (a) Three-dimensional FE-SEM images of GaN NWs. Inset: plan-view image. (b) TEM (left) and HR-TEM (middle) image and SAED patterns (right) of a single GaN NW measured at two different vertical positions. (c) XRD rocking curve and (d) PL spectrum of GaN NWs.

an interlocked nanoridge structure to transfer external stress to the underlying GaN NWs. The first step of the device fabrication entailed mixing the silicone elastomer with the curing agent by mechanically stirring for 10 minutes to form a PDMS mixture. This mixture was degassed in a vacuum desiccator for 30 minutes to remove air bubbles, whereupon the mixture was uniformly spin-coated on a glass substrate at 600 rpm for 40 s. The mixture was placed in an oven for an hour at 70 °C to affect solidification. Subsequently, the PDMS film was peeled off from the glass substrate. Then, Pt was deposited as an electrode underneath the Si(111) substrate on which the GaN NWs were grown, and a Cu electrode was additionally connected. As the last step, the TES was fabricated by stacking PDMS directly on the GaN NWs on the Si(111) substrate with the Pt/Cu electrode.

Fig. 3(a) illustrate the device structure of the TES based on the interlocked nanoridge structure at the interface between the GaN NWs and PDMS. The role of each layer was systematically evaluated by fabricating devices with the structures of only Si (TES1), PDMS/Si (TES2), and PDMS/GaN-NWs/Si (TES3). The electrical properties of the TESs were measured by periodically bringing the top surface of the TES devices into contact with a human finger. Fig. 3(b) shows the output voltages of the TESs with different device structures as a function of time. The maximum output voltages of the TES1, TES2, and TES3 samples were measured to be 1.2 V, 6.6 V, and 14.7 V, respectively. Among the TES samples, the highest output voltage was measured for the TES3. Considering the representative results listed in Table 1, the output voltage of TES3 is much higher than those reported for previous studies.[34–38] This is attributed to the induction of a high triboelectric charge resulting from the high-crystalline WZ structure of the GaN NWs and the interlocked nanoridge structure formed by the PDMS layer. For the touch sensor, triboelectric effect is often combined with the piezoelectric effect when contacting devices.[39] To distinguish which of the two components is the main operation mechanism for our devices, the time-dependent output voltage of the TES is expanded as shown in Fig. 3(c). There are three peaks with the voltage values of 15.4, 3.1, and (−)15.1 V. In the previous reports on touch sensors based on triboelectric effect, there were three distinct peaks corresponding to touching, pressing, and releasing process, where the piezoelectric component was negligibly small.[40] Similarly, the three peaks in this work correspond to the moments of touching, applying pressure, and releasing the finger from the TES surface, respectively.[5,39] That is, the peaks with the voltage values of 15.4 and 3.1 V are attributed to the triboelectric and piezoelectric effects, respectively. The peak

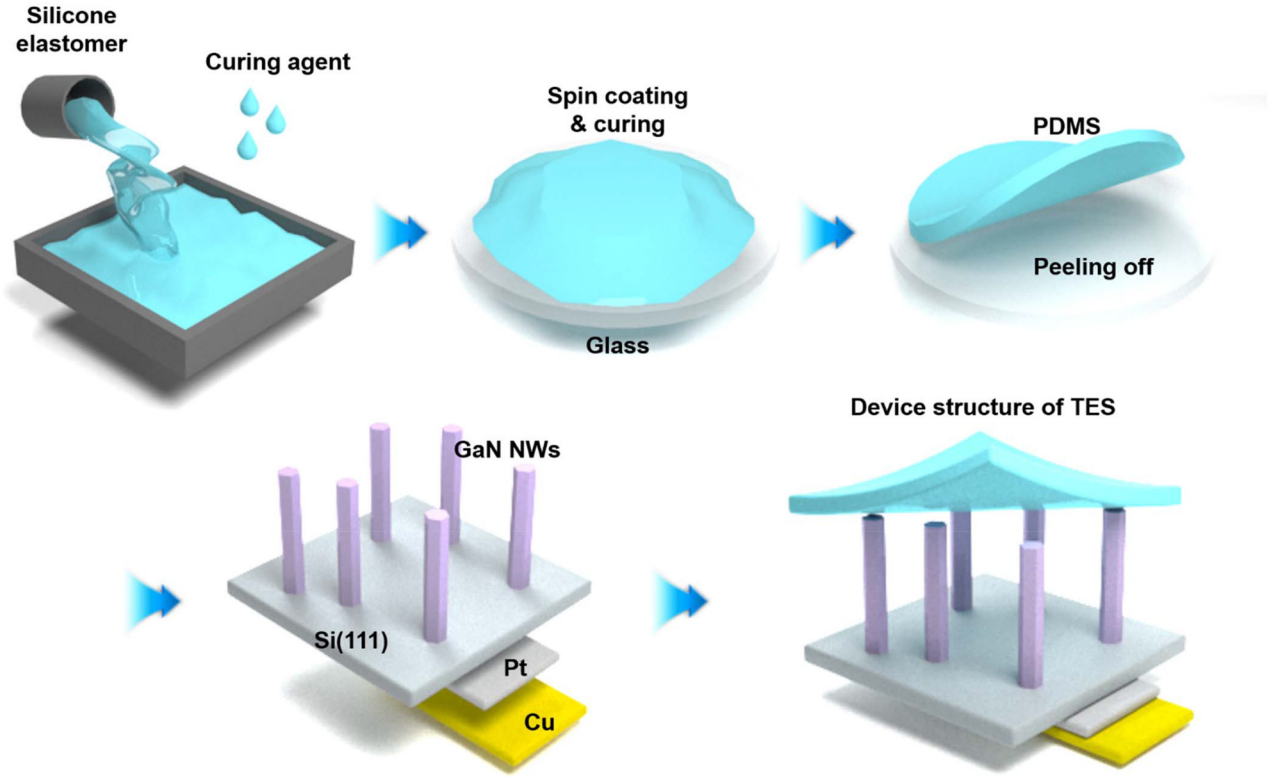

Fig. 2 Schematic diagram of the fabrication process of TES using GaN NWs and PDMS.

intensity related to piezoelectric effect is much smaller than that related to the triboelectric effect. In addition, M. Ha *et al.* reported that the performance of the touch sensor with the interlocked microridge structure is related to the triboelectric effect.[41] The nanoridge structure of our TES devices is similar to the microridge structure. Considering the expanded plot of the output voltage and previous reports, the triboelectric effect is dominant operation mechanism for the TES with GaN NWs. Fig. 3(d) illustrate the device structure of the TES and operating mechanism based on the interlocked nanoridge structure at the interface between the GaN NWs and PDMS. The TES device in this work mimics the structure of human skin, which is characterized by a stiffness gradient between the stiff epidermis and soft dermis.[42] This gradient facilitates the transfer and concentration of effective stress to the underlying layer. As evident from the device structure of the TES in Fig. 3(d), the interlocked nanoridge structure is the result of using the soft PDMS layer in combination with the stiff GaN NWs. The color scale is representative of the extent of charge separation, with red and blue indicating negative and positive charges, respectively. When the top surface of the TES is touched with a human finger, the interlocked nanoridge structures are spatially generated between the upper PDMS layer with its relatively low elastic modulus and the lower GaN NW layer with its relatively high elastic modulus and the contact electrification simultaneously occurs.[39] The stiffness gradient, which arises because of the difference in the elastic moduli between the GaN NWs and PDMS, effectively transfers and concentrates the stress on the GaN NWs to generate triboelectricity.[43] The triboelectric charge density provided by this device structure is approximately 1.5 times higher than that of the TES without the structure. The electricity generated by the TES can be calculated, by defining the electric field by the following equation:[44]

$$E = -\frac{(Q - A\sigma(t))}{A\varepsilon_0\varepsilon_r} \quad (1)$$

where E is the electric field, Q is the amount of surface charge, A is the area of electrode, σ is the triboelectric charge density, ε_0 is the permittivity of air, and ε_r is the permittivity of each of the two components, the GaN NWs and PDMS. Therefore, the triboelectric voltage in the contact-separation mode of the TES device can be derived as follows:

$$\begin{aligned} V &= E_{GaN}T_{GaN} + E_{PDMS}T_{PDMS} + E_{air}d \\ &= -\frac{Q}{A\varepsilon_0}\left(\frac{T_{GaN}}{\varepsilon_{r,GaN}} + \frac{T_{PDMS}}{\varepsilon_{r,PDMS}} + d(t)\right) + \frac{\sigma d(t)}{\varepsilon_0} \end{aligned} \quad (2)$$

where T_{GaN}, T_{PDMS}, and d are the thicknesses of the GaN NW and PDMS layers, and the air gap distance, respectively. Because the TES device in this work is operated under open-circuit conditions, charge transfer does not occur. Therefore, the term representing the charges can be eliminated to yield the proportional relationship between the triboelectric voltage

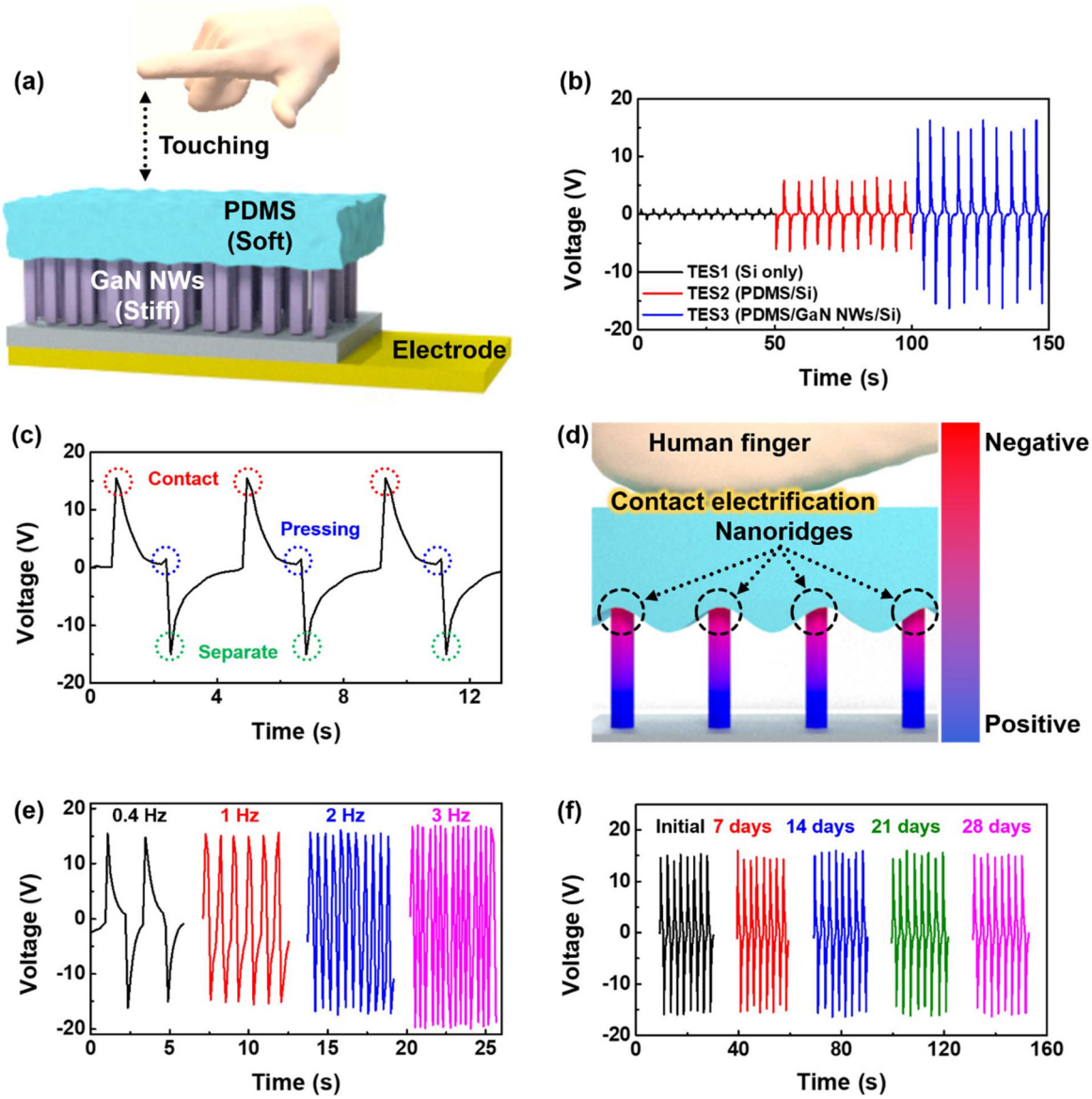

Fig. 3 (a) Schematic diagram of the TES device. (b) Output voltages of TESs with different device structures as a function of time. (c) The output voltages when the top surface of the TES is contacted, pushed, and separated with a human finger. (d) Schematic diagram of the operating mechanism using the interlocked nanoridge structure composed of the GaN NWs and PDMS layer. (e) Output voltages of the TES with the touching frequency. (f) The output voltages of the TES measured immediately, and 7, 14, 21, and 28 days after the device fabrication.

Table 1 Summary of representative results of TESs with various materials

Materials	Output voltage [V]	Power density [mW m^{-2}]	Ref.
Styrene rubber/PDMS	0.012	—	34
PDMS/PFA/Ag NWs/ITO	4	—	35
ZnS nanosheets/PDMS	8	4.33	36
MXene/PDMS	2.3	—	37
Silicone elastomer/PET	5.5	17.1	38
PDMS/GaN NWs	14.7	63.7	This work

and charge density. Considering the structure of the TES devices and the interface between the GaN NWs and PDMS, the stress is concentrated at the top of the GaN NWs. As mentioned above, this stress concentration in the GaN NWs can increase the triboelectric charge density to amplify the voltage. Fig. 3(e) shows the output voltage of TES3, measured by

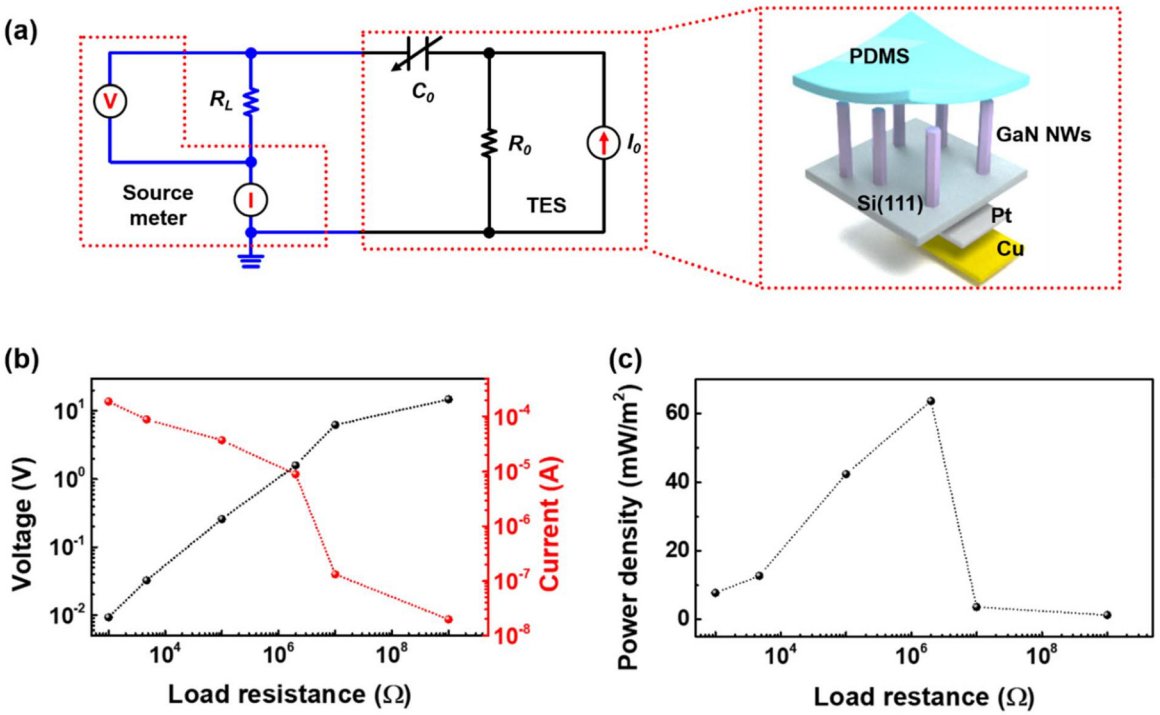

Fig. 4 (a) Simplified equivalent circuit model connected with a source meter and the layout of the TES. (b) Summary of average output voltage and current of the TES as a function of R_L. (c) Calculated power density of the TES as a function of R_L.

varying the touching frequency from 0.4 to 3 Hz. As the touching frequency increases, the maximum output voltage increases slightly. This result can be explained by the presence of residual charges caused by incomplete electrical neutralization during measurement, which leads to an elevation in the triboelectric potential. Fig. 3(f) shows the time-dependent output voltage of the TES measured for 28 days. The average output voltages measured immediately, and 7, 14, 21, and 28 days after the device fabrication were observed to be 15.3, 14.6, 15.5, 15.2, and 14.9 V, respectively. There is no significant degradation in the device performance over time, indicating long-term stable operation of the TES.

To measure the triboelectric voltages of the device with the source meter, the Pt/Cu electrode was connected to a load resistance ranging from 1 kΩ to 1 GΩ. Fig. 4(a) shows the simplified equivalent circuit connected with a source meter and the layout of equivalent circuit connected with a source meter and the layout of the TES. The TES can be approximated as an equivalent circuit with a current source (I_0), internal resistance (R_0), and internal capacitance (C_0) in terms of electrical signals. Fig. 4(b) summarizes on the maximum output voltages and currents of the TES3 device as a function of R_L. An increase in R_L gave rise to a linear increase in the output voltage. The instantaneous current decreases with increasing R_L due to the occurrence of Ohmic loss while the voltage increases. Fig. 4(c) shows the power density of TES3 as a function of R_L, calculated from the output voltages and currents. The power density increased up to the R_L of 2 MΩ, at which the power density reached the maximum value of 63.7 mW m^{-2}. Considering the representative results listed in Table 1, the power density of TES3 is much higher than those of the TESs in previous studies.[36,38] A further increase the R_L caused the power density to decrease because of ohmic loss.

Conclusions

In summary, we successfully developed a self-powered TES with an interlocked nanoridge structure that was inspired by the structure of human skin. The TES device includes GaN NWs underneath a PDMS layer. The TESs with the interlocked nanoridge structures were fabricated by stacking PDMS directly on the GaN NWs on the Si(111) substrate. The PDMS layer forms an interlocked nanoridge structure at the interface with the top surface of GaN NWs. The maximum output voltage and power density when the upper surface of the TES with the GaN NWs is touched with a human finger reaches 14.7 V and 63.7 mW m^{-2}, respectively. These values are much higher than those of previously reported TESs. The outstanding device performance of the TES incorporating the GaN NWs is attributed to the enhanced spatial electrostatic induction at the GaN NWs due to the effective transfer and concentration of stress to the GaN NWs using the skin-inspired interlocked nanoridge structure formed by the PDMS layer.

Author contributions

J. S. K. designed the research project and supervised the experiments. S. N., J. S., S. J., S. K., and Y. L. performed the experiments and analysed the data. J. S. K. and S. N. wrote the paper, which was discussed by all the authors.

Data availability

Data that support the findings of this study are available from the corresponding author (Jin Soo Kim) upon reasonable request.

Conflicts of interest

There are no conflicts to declare.

Acknowledgements

This work was supported in part by the National Research Foundation of Korea (NRF) funded by the Ministry of Education (No. 2023R1A2C1005913), by the Civil-Military Technology Cooperation Program (No. 19-CM-BD-05), and by BK21 FOUR Program by Jeonbuk National University Research Grant.

References

1 M. Lin, H. Hu, S. Zhou and S. Xu, Soft wearable devices for deep-tissue sensing, *Nat. Rev. Mater.*, 2022, **7**, 850–869.
2 S. R. Menaka, M. Prakash, S. Neelakanadan and A. Radhakrishnan, A novel WGF-LN based edge driven intelligence for wearable devices in human activity recognition, *Sci. Rep.*, 2023, **13**, 17822.
3 Y. J. Jeon, S. H. Park and S. J. Kang, Self-x based closed loop wearable IoT for real-time detection and resolution of sleep apnea, *Internet Things*, 2023, **22**, 100767.
4 C. Hou, Z. Xu, W. Qiu, R. Wu, Y. Wang, Q. Xu, X. Y. Liu and W. Guo, A biodegradable and stretchable protein – based sensor as artificial electronics skin for human motion detection, *Small*, 2019, **15**, 1805084.
5 H. Niu, H. Li, S. Gao, Y. Li, X. Wei, Y. Chen, W. Yue, W. Zhou and G. Shen, Perception-to-cognition tactile sensing based on artificial-intelligence-motivated human full-skin bionic electronic skin, *Adv. Mater.*, 2022, **34**, 2202622.
6 T. An, D. V. Anaya, S. Gong, L. W. Yap, F. Lin, R. Wang, M. R. Yuce and W. Cheng, Self-powered gold nanowire tattoo triboelectric sensors for soft wearable human-machine interface, *Nano Energy*, 2020, **77**, 105295.
7 D. V. Anaya, T. He, C. Lee and M. R. Yuce, Self-powered eye motion sensor based on triboelectric interaction and near-field electrostatic induction for wearable assistive technologies, *Nano Energy*, 2020, **72**, 104675.
8 X. Xiong, J. Liang and W. Wu, Principle and recent progress of triboelectric pressure sensors for wearable applications, *Nano Energy*, 2023, **113**, 108542.
9 Y. Zhong, J. Wang, L. Wu, K. Liu, S. Dai, J. Hua, G. Cheng and J. Ding, Dome-conformal electrode strategy for enhancing the sensitivity of $BaTiO_3$-doped Flexible self-powered triboelectric pressure sensor, *ACS Appl. Mater. Interfaces*, 2023, **16**, 1727–1736.
10 M. Cao, J. Su, S. Fan, H. Qiu, D. Su and L. Li, Wearable piezoresistive pressure sensors based on 3D graphene, *Chem. Eng. J.*, 2021, **406**, 126777.
11 G. Hossain, I. Z. Hossain and G. Grabher, Piezoresistive smart-textile sensor for inventory management record, *Sens. Actuators, A*, 2020, **315**, 112300.
12 J. Qin, L.-J. Yin, Y.-N. Hao, S.-L. Zhong, D.-L. Zhang, K. Bi, Y.-X. Zhang, Y. Zhao and Z.-M. Dang, Flexible and stretchable capacitive sensors with different microstructures, *Adv. Mater.*, 2021, **33**, 2008267.
13 S. R. A. Ruth, V. R. Feig, M.-G. Kim, Y. Khan, J. K. Phong and Z. Bao, Flexible fringe effect capacitive sensors with simultaneous high–performance contact and non–contact sensing capabilities, *Small Struct.*, 2021, **2**, 2000079.
14 E. S. Hosseini, L. Manjakkal, D. Shakthivel and R. Dahiya, Glycine–chitosan-based flexible biodegradable piezoelectric pressure sensor, *ACS Appl. Mater. Interfaces*, 2020, **12**, 9008–9016.
15 C. Zhi, S. Shi, Y. Si, B. Fei, H. Huang and J. Hu, Recent progress of wearable piezoelectric pressure sensors based on nanofibers, yarns, and their fabrics via electrospinning, *Adv. Mater. Technol.*, 2023, **8**, 2201161.
16 S. Chen, S. Xin, L. Yang, Y. Guo, W. Zhang and K. Sun, Multi-sized planar capacitive pressure sensor with ultra-high sensitivity, *Nano Energy*, 2021, **87**, 106178.
17 H. Li, K. Wu, Z. Xu, Z. Wang, Y. Meng and L. Li, Ultrahigh-sensitivity piezoresistive pressure sensors for detection of tiny pressure, *ACS Appl. Mater. Interfaces*, 2018, **10**, 20826–20834.
18 N. Yogeswaran, E. S. Hosseini and R. Dahiya, Graphene based low voltage field effect transistor coupled with biodegradable piezoelectric material based dynamic pressure sensor, *ACS Appl. Mater. Interfaces*, 2020, **12**, 54035–54040.
19 J. Wang, S. Qian, J. Yu, Q. Zhang, Z. Yuan, S. Sang, X. Zhou and L. Sun, Flexible and wearable PDMS-based triboelectric nanogenerator for self-powered tactile sensing, *Nanomaterials*, 2019, **9**, 1304.
20 Y. Wang, X. Yang, X. Yu, J. Duan, Q. Yang, Y. Duan and Q. Tang, Triboelectric charging behaviors and photo-induced enhancement of alkaline earth ions doped inorganic perovskite triboelectric nanogenerators, *Nano Energy*, 2020, **77**, 105280.
21 B.-B. Yu, X. Hu, H. Wang, Q. Liang, L. Wang, Y. Wu, Q. Qin and L.-B. Huang, Improved perovskite triboelectric nanogenerators by effective defect passivation and interface modulation, *Appl. Phys. Lett.*, 2023, **122**, 133902.

22 M. Yang, H. Shu, P. Tang, P. Liang, D. Cao and X. Chen, Intrinsic polarization-induced enhanced ferromagnetism and self-doped p–n junctions in $CrBr_3$/GaN van der Waals heterostructures, *ACS Appl. Mater. Interfaces*, 2021, **13**, 8764–8773.
23 M. Kammermeier, A. Seith, P. Wenk and J. Schliemann, Persistent spin textures and currents in wurtzite nanowire-based quantum structures, *Phys. Rev. B*, 2020, **101**, 195418.
24 J. Shin, S. Noh, J. Lee, J. Oh, M.-Y. Ryu and J. S. Kim, Structural and Optical Properties of InN Nanowires Formed on Si (111), *Appl. Sci. Convergence Technol.*, 2022, **31**, 141–144.
25 E. Monaico, C. Moise, G. Mihai, V. V. Ursaki, K. Leistner, I. M. Tiginyanu, M. Enachescu and K. Nielsch, Towards uniform electrochemical porosification of bulk HVPE-grown GaN, *J. Electrochem. Soc.*, 2019, **166**, H3159–H3166.
26 R. Chen, J. Liu, B. Feng, H. Zhu, D. Wang, C. Luan, J. Ma, L. Zhang and H. Xiao, Pores in p-type GaN by annealing under nitrogen atmosphere: formation and photodetector, *J. Mater. Sci.*, 2022, **57**, 467–476.
27 S. Noh, S. Han, J. Shin, J. Lee, I. Choi, H. M. Oh, M.-Y. Ryu and J. S. Kim, Photoelectrochemical water splitting using GaN nanowires with reverse-mesa structures as photoanode material, *Appl. Sci. Convergence Technol.*, 2022, **31**, 51–55.
28 S. Noh, J. Shin, J. Lee, H. M. Oh, Y.-T. Yu and J. S. Kim, Improvement in Photoelectrochemical Water Splitting Performance of GaN-nanowire Photoanode Using MXene, *ACS Appl. Mater. Interfaces*, 2024, **16**, 8016–8023.
29 M. Maraj, G. Nabi, K. Usman, E. Wang, W. Wei, Y. Wang and W. Sun, High quality growth of cobalt doped GaN nanowires with enhanced ferromagnetic and optical response, *Materials*, 2020, **13**, 3537.
30 A. Wierzbicka, G. Tchutchulashvili, M. Sobanska, K. Klosek, R. Minikayev, J. Z. Domagala, J. Borysiuk and Z. R. Zytkiewicz, Arrangement of GaN nanowires on Si (001) substrates studied by X-ray diffraction: Importance of silicon nitride interlayer, *Appl. Surf. Sci.*, 2017, **425**, 1014–1019.
31 M. Junaid, C.-L. Hsiao, Y.-T. Chen, J. Lu, J. Palisaitis, P. O. A. Persson, L. Hultman and J. Birch, Effects of N_2 partial pressure on growth, structure, and optical properties of GaN nanorods deposited by liquid-target reactive magnetron sputter epitaxy, *Nanomaterials*, 2018, **8**, 223.
32 X. Yang, A. Jena, F. Meng, S. Wen, J. Ma, X. Li and W. Li, Indirect electron-phonon interaction leading to significant reduction of thermal conductivity in graphene, *Mater. Today Phys.*, 2021, **18**, 100315.
33 H. Lee, Theoretical study on electronic structure and charge transport characteristics of anthracene-based host material for blue organic light-emitting diode application, *Appl. Sci. Convergence Technol.*, 2018, **27**, 161–165.
34 H. J. Lee, K.-Y. Chun, J. H. Oh and C.-S. Han, Wearable triboelectric strain-insensitive pressure sensors based on hierarchical superposition patterns, *ACS Sens.*, 2021, **6**, 2411–2418.
35 S. Lee and J.-W. Park, Fingerprint-inspired triboelectric nanogenerator with a geometrically asymmetric electrode design for a self-powered dynamic pressure sensor, *Nano Energy*, 2022, **101**, 107546.
36 S. Mishra, S. Potu, R. S. Puppala, R. K. Rajaboina, P. Kodali and H. Divi, A novel ZnS nanosheets-based triboelectric nanogenerator and its applications in sensing, self-powered electronics, and digital systems, *Mater. Today Commun.*, 2022, **31**, 103292.
37 Z. Wang, Z. Xu, N. Li, T. Yao and M. Ge, Flexible pressure sensors based on MXene/PDMS porous films, *Adv. Mater. Technol.*, 2023, **8**, 2200826.
38 V. Vivekananthan, A. Chandrasekhar, N. R. Alluri, Y. Purusothaman and S. J. Kim, A highly reliable, impervious and sustainable triboelectric nanogenerator as a zero-power consuming active pressure sensor, *Nanoscale Adv.*, 2020, **2**, 746–754.
39 C. Chen, S. Zhao, C. Pan, Y. Zi, F. Wang, C. Yang and Z. L. Wang, A method for quantitatively separating the piezoelectric component from the as-received "Piezoelectric" signal, *Nat. Commun.*, 2022, **13**, 1391.
40 W.-S. Jung, M.-G. Kang, H. G. Moon, S.-H. Baek, S.-J. Yoon, Z.-L. Wang, S.-W. Kim and C.-Y. Kang, High output piezo/triboelectric hybrid generator, *Sci. Rep.*, 2015, **5**, 9309.
41 M. Ha, S. Lim, S. Cho, Y. Lee, S. Na, C. Baig and H. Ko, Skin-inspired hierarchical polymer architectures with gradient stiffness for spacer-free ultrathin, and highly sensitive triboelectric sensors, *ACS Nano*, 2018, **12**, 3964–3974.
42 Y. Ma, J. Cao, S. Li, L. Wang, Y. Meng and Y. Chen, Nature-inspired wet drug delivery platforms, *Small Methods*, 2024, 2301726.
43 Y. Cao, Y. Feng, M. D. Ryser, K. Zhu, G. Herschlag, C. Cao, K. Marusak, S. Zauscher and L. You, Programmable assembly of pressure sensors using pattern-forming bacteria, *Nat. Biotechnol.*, 2017, **35**, 1087–1093.
44 S. Niu, S. Wang, L. Lin, Y. Liu, Y. S. Zhou, Y. Hu and Z. L. Wang, Theoretical study of contact-mode triboelectric nanogenerators as an effective power source, *Energy Environ. Sci.*, 2013, **6**, 3576–3583.